Electronic Supplementary Material (ESI) for Journal of Materials Chemistry A.

Supporting Information

Ultrathin CoO_x Nanolayers Derived from Polyoxometalate for Enhanced Photoelectrochemical Performance of Hematite Photoanodes

Xiaohu Cao,[a] Yifan Wang,[a] Junqi Lin[a], Yong Ding*,[a,b]

[a] State Key Laboratory of Applied Organic Chemistry, Key Laboratory of Nonferrous Metals Chemistry and Resources Utilization of Gansu Province, and College of Chemistry and Chemical Engineering, Lanzhou University, Lanzhou 730000, China

[b] State Key Laboratory for Oxo Synthesis and Selective Oxidation, Lanzhou Institute of Chemical Physics, Chinese Academy of Sciences, Lanzhou 730000, China
*E-mail: dingyong1@lzu.edu.cn

Synthesis of $Na_{10}[A\text{-}\alpha\text{-}SiW_9O_{34}]\cdot 19H_2O$

$Na_2WO_4\cdot 2H_2O$ (36.4 g) and $Na_2SiO_3\cdot 5H_2O$ (2.2 g) were dissolved in 40 mL of hot water (80-100 ℃). Then, this solution was added dropwise 26 mL of 6 M HCl in ~30 min with vigorous stirring. The solution was boiled until the volume is ~60 mL and filtrated. Na_2CO_3 (10 g) was dissolved in 30 mL water and slowly added to the above filtrate with gentle stirring. A precipitate formed slowly and was filtrated after ~1 h. The solid was stirred with 200 mL of 4 M NaCl solution and filtrated again. It was then washed successively with two 50-mL portions of ethanol and 50 mL of diethyl ether and dried under vacuum.

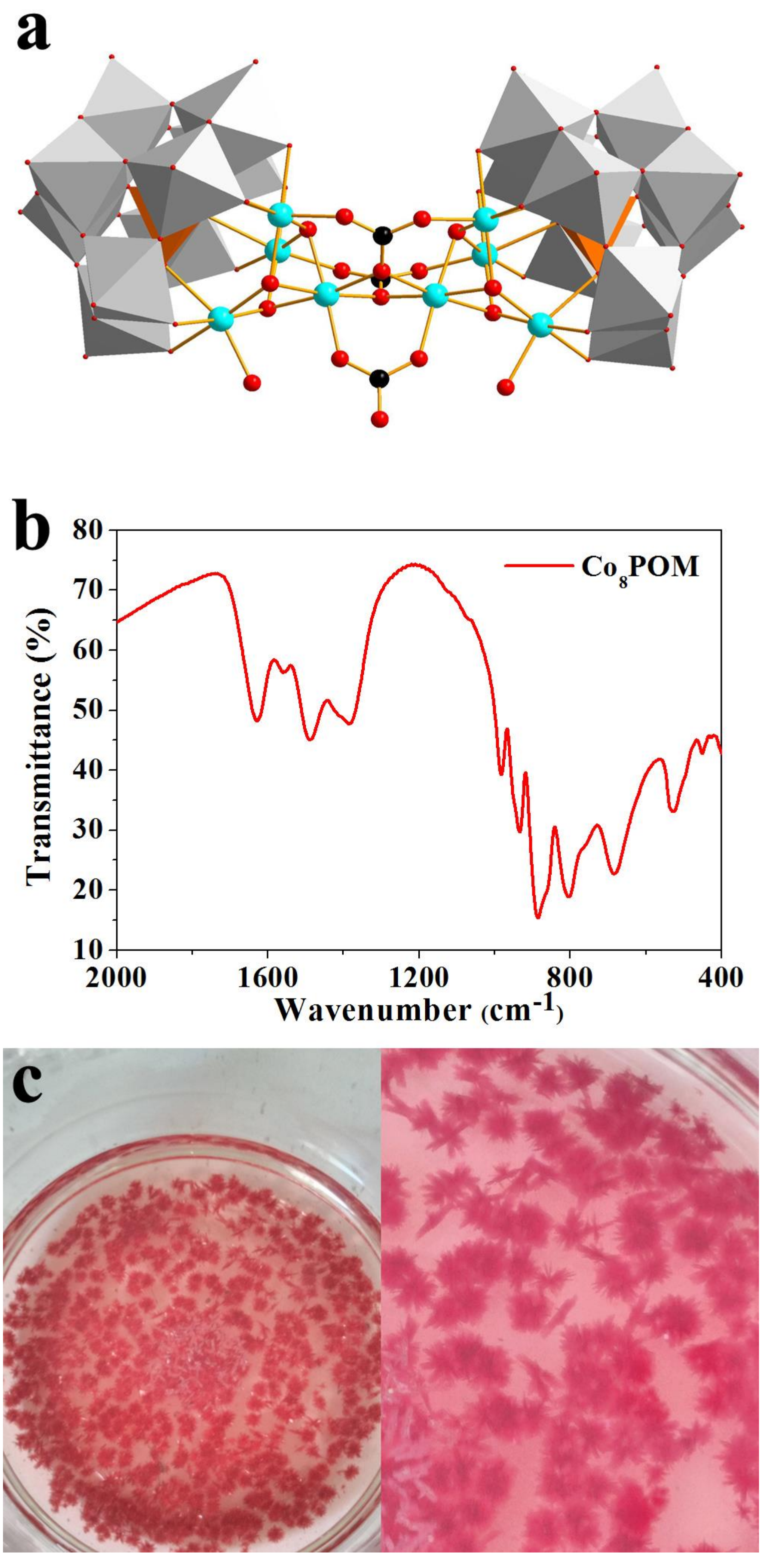

Figure S1. (a) X-ray crystal structure of Co$_8$POM in combined ball-and-stick and polyhedral representation (Co, cyan; O, red; Si, orange; C, black; W, gray; counter cations and H atoms were omitted for clarity). (b) FT-IR spectrum of Co$_8$POM. (c) Images of crystal Co$_8$POM

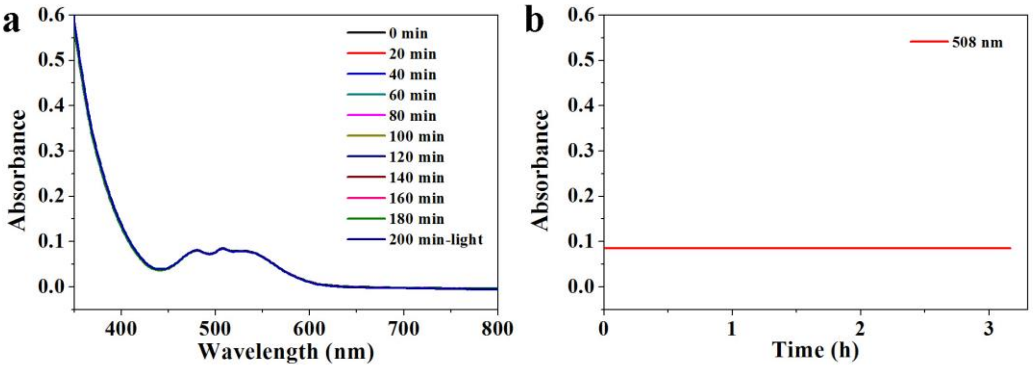

Figure S2. (a) Time-dependent UV-Vis absorption spectra of Co_8POM (0.5 mM). 200 min-light means that the sample was treated by illumination for 20 min (AM 1.5G, 100 mW/cm^2) at the end. (b) Kinetic trace at 508 nm according to the local maximum of Co_8POM in the UV-visible spectrum over a 3 h period (less than 1% decrease). These results illustrate the good stability of Co_8POM in the borate buffer solution (pH 9).

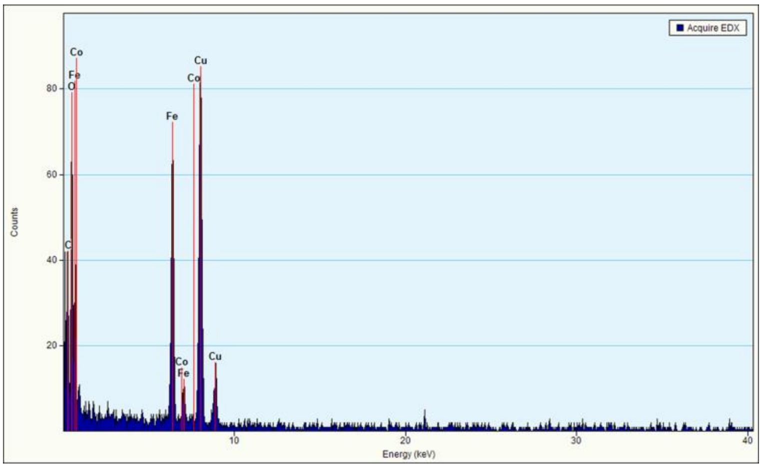

Figure S3. EDX of $CoO_x(POM)/Fe_2O_3$ photoanode. Cu element belongs to the substrate for TEM characterization. Tungsten (W) and silicon (Si) elements, which account for a significant proportion in Co_8POM, are not detected by EDX. It indicates that W and Si are not obviously affected by photo-generated carriers.

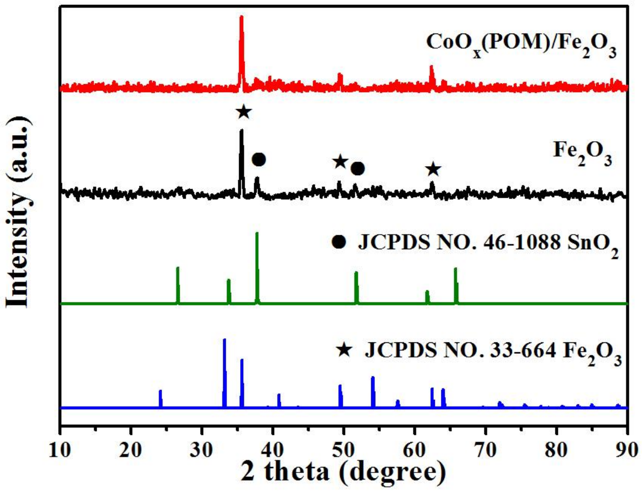

Figure S4. XRD patterns of pristine Fe_2O_3 and CoO_x(POM)/Fe_2O_3 photoanodes measured at a small grazing angle (Omega=0.5).

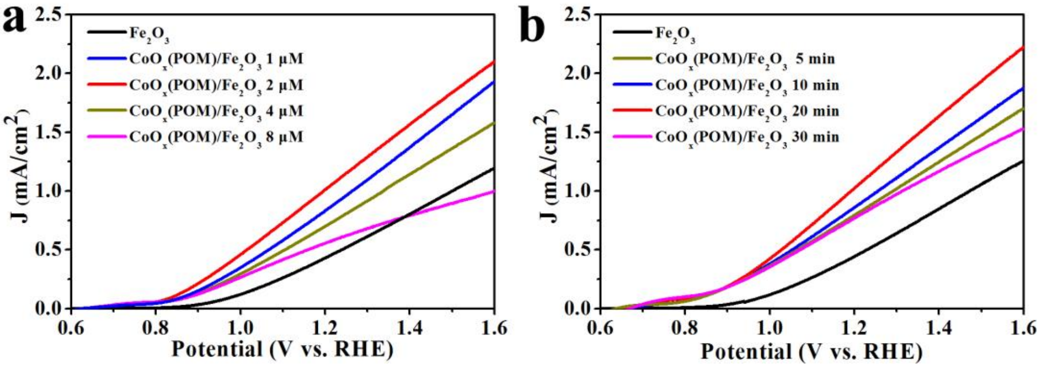

Figure S5. Optimizations with various Co_8POM concentrations (all in 20 min) (a) as well as various illumination times (all in 2 μM) (b) for photodeposition treatments in Co_8POM solutions.

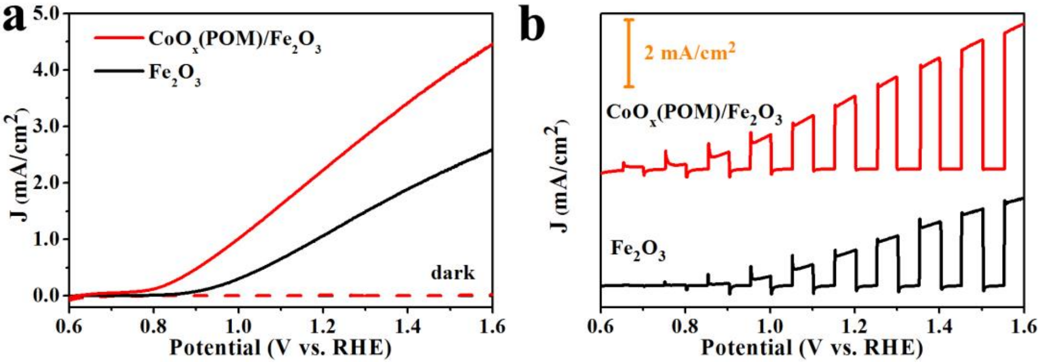

Figure S6. LSV (a) and chop LSV (b) of $CoO_x(POM)/Fe_2O_3$ and Fe_2O_3 photoanodes at 1 M NaOH (pH 13.6) electrolyte. For the original intention of investigating true active species, an 80 mM borate buffer solution (pH 9) was performed for almost all measurements in this paper.[1] For comparison, 1 M NaOH solution (pH 13.6), the most commonly used electrolyte for hematite photoanodes, was also applied as the electrolyte for the $CoO_x(POM)/Fe_2O_3$ electrode. Herein, the photocurrent arrived at 2.4 mA/cm^2 at 1.23 V_{RHE} which is twice as high as that of pristine hematite photoanode (1.2 mA/cm^2). It strongly confirmed that our CoO_x cocatalyst prepared by a simple photodeposition method is comparable to other Co-based cocatalysts (Table S1). As shown in Figure S7, the photocurrent density of a piece of hematite photoanode differs from electrolyte to electrolyte.

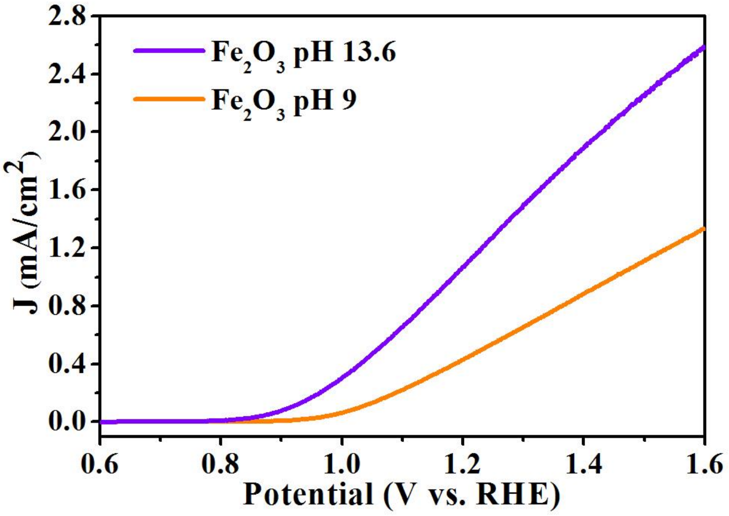

Figure S7. A piece of pristine Fe_2O_3 photoanode was tested by LSV in different electrolytes (pH 9 borate buffer solution and pH 13.6 NaOH electrolyte).

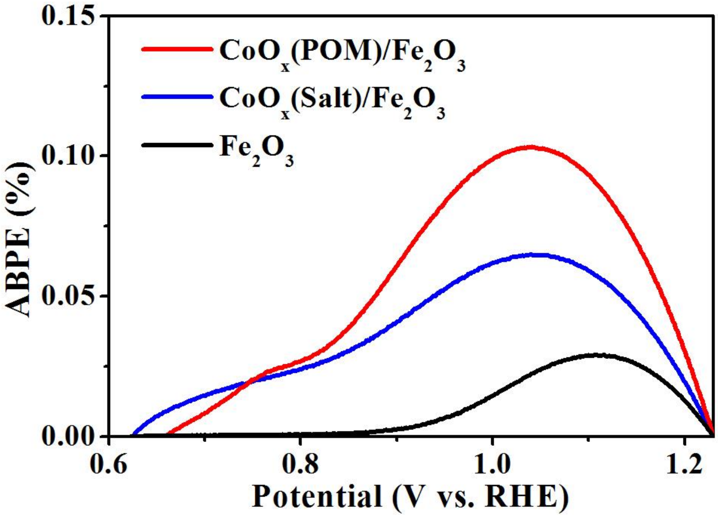

Figure S8. Applied bias photon-to-current efficiencies (ABPE) of CoO$_x$(POM)/Fe$_2$O$_3$, CoO$_x$(Salt)/Fe$_2$O$_3$, and Fe$_2$O$_3$ photoanodes.

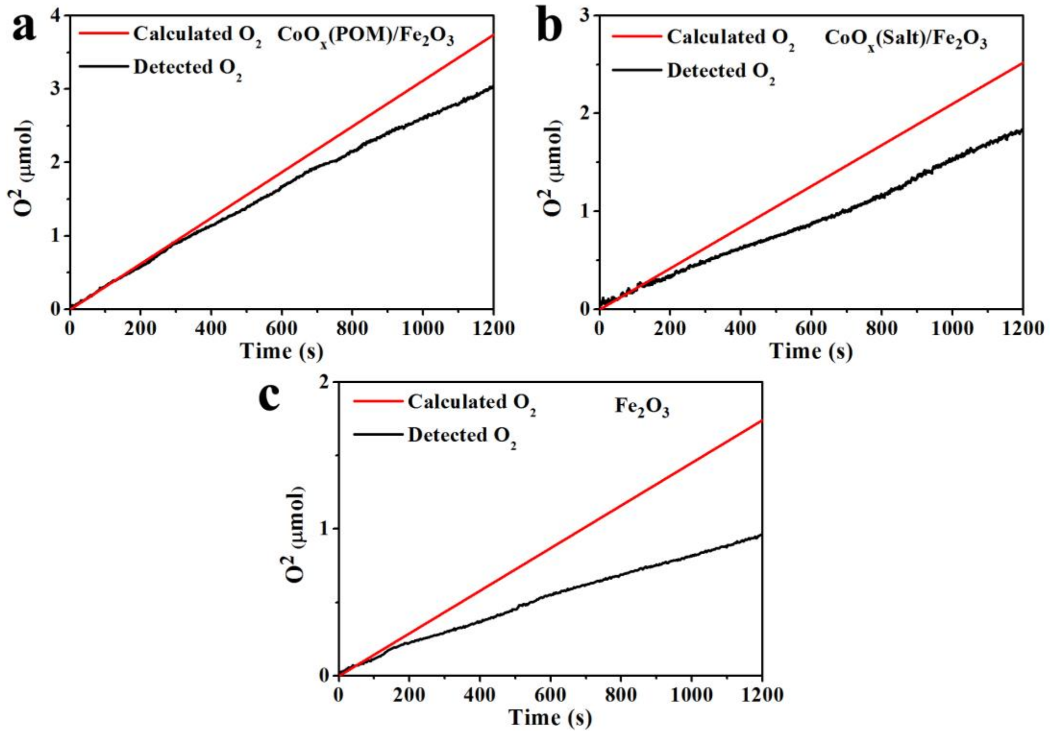

Figure S9. Generated oxygen monitored by a Clark electrode in the PEC experiment. The potential is controlled at 1.23 V vs. RHE. The Faradaic efficiencies of (a) CoO_x(POM)/Fe_2O_3, (b) CoO_x(Salt)/Fe_2O_3 and (c) Fe_2O_3photoanodes are 81.9%, 72.6% and 55.2%.

The Clark electrode can detect dissolved oxygen in liquid phase. Before experiment, the air in both liquid phase and head vial is removed by bubbling Ar gas and the electrolyte is covered by a layer of cyclohexane to prohibit the diffusion of produced oxygen from electrolyte. Despite of the pretreatments, it is impossible to completely prevent oxygen from escaping as time goes on. The real amount of O_2 is therefore underestimated to a certain extent.

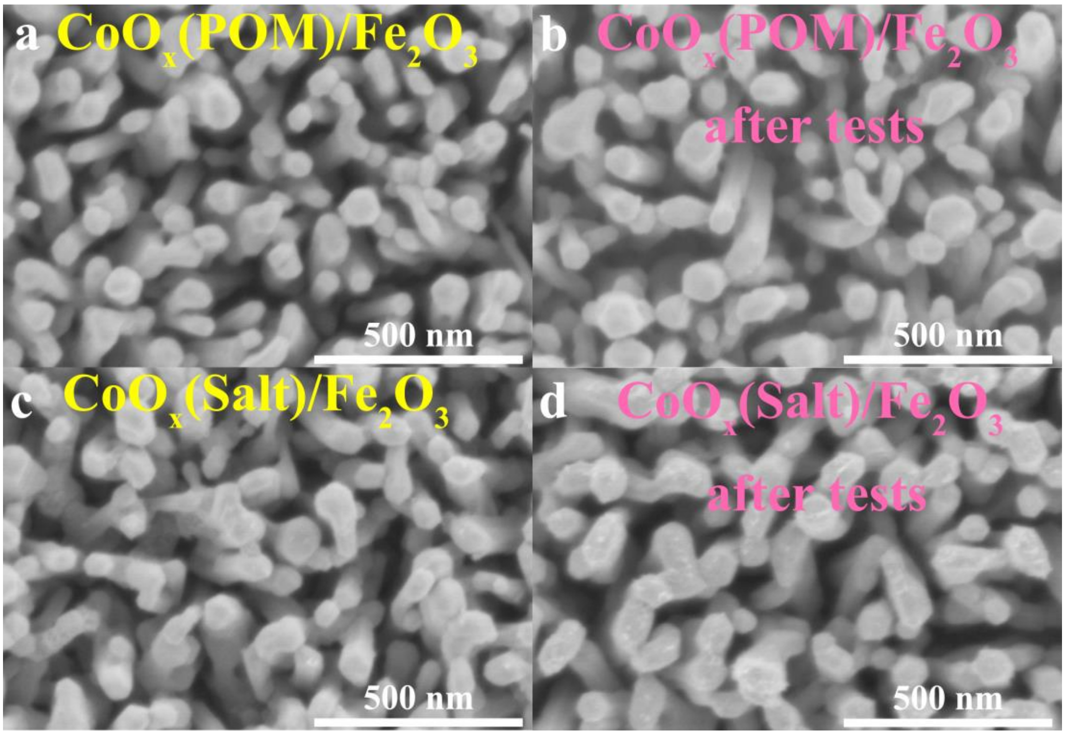

Figure S10. SEM of CoO_x(POM)/Fe_2O_3 photoanode before (a) and after (b) PEC tests, CoO_x(Salt)/Fe_2O_3 photoanode before (c) and after (d) PEC tests. It can be observed that the surface morphology of CoO_x(Salt)/Fe_2O_3 has a change before and after PEC tests.

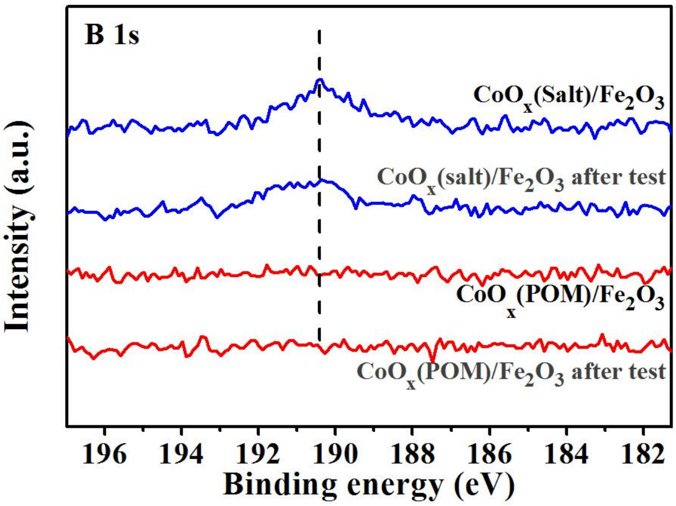

Figure S11. B 1s spectra of CoO_x(POM)/Fe_2O_3 and CoO_x(Salt)/Fe_2O_3 photoanodes before and after PEC tests. It is a solid evidence that different Co-based cocatalysts were fabricated on hematite photoanodes derived from different cobalt sources. CoB_i species is observed on CoO_x(Salt)/Fe_2O_3 photoanode but not on CoO_x(POM)/Fe_2O_3 photoanode.

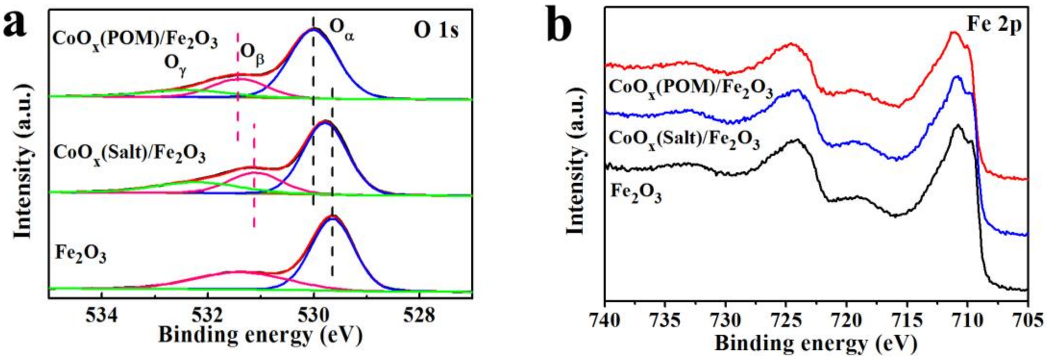

Figure S12. (a) O 1s and (b) Fe 2p spectra of CoO$_x$(POM)/Fe$_2$O$_3$, CoO$_x$(Salt)/Fe$_2$O$_3$, and Fe$_2$O$_3$ photoanodes. The O 1s high-resolution spectra can be decomposed into three peaks for both pristine and composite photoanodes [2](designated as O$_\alpha$, O$_\beta$ and O$_\gamma$). The peak at low binding energy is characteristic of metal oxide (O$_\alpha$), while the other two peaks are associated with hydroxide species (O$_\beta$) and adsorbed molecular water (O$_\gamma$)[3, 4]. After coating with Co-based nanolayers in CoO$_x$(POM)/Fe$_2$O$_3$ and CoO$_x$(Salt)/Fe$_2$O$_3$ electrodes, the peaks of O$_\alpha$ are positively shifted, suggesting the change of binding environment caused by cocatalyst overlayers. Meanwhile, the peak of O$_\beta$ in CoO$_x$(POM)/Fe$_2$O$_3$ locates at higher binding energy than that of CoO$_x$(Salt)/Fe$_2$O$_3$. It indicates that CoO$_x$(POM)/Fe$_2$O$_3$ electrode contains more cobalt (oxy)hydroxide than CoO$_x$(Salt)/Fe$_2$O$_3$ electrode which mainly contains CoB$_i$ species.

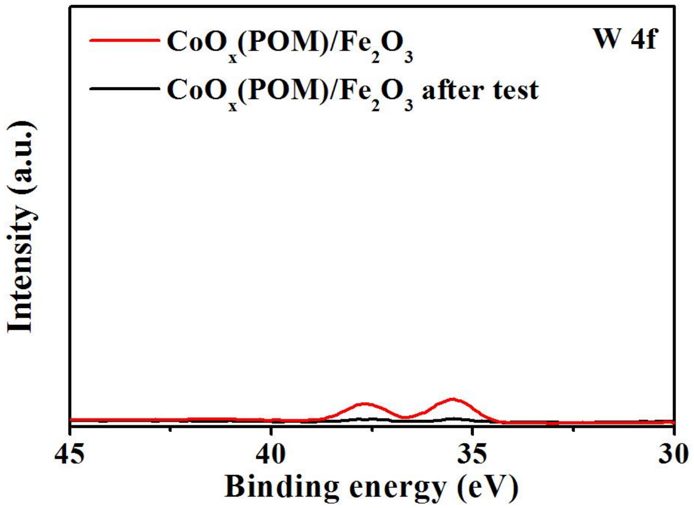

Figure S13. W 4f spectra of CoO$_x$(POM)/Fe$_2$O$_3$ photoanodes before and after PEC tests (over 3h tests). The apparent reduction of XPS signal after PEC tests illustrates that the tiny amount of W element may be as a result of adsorption.

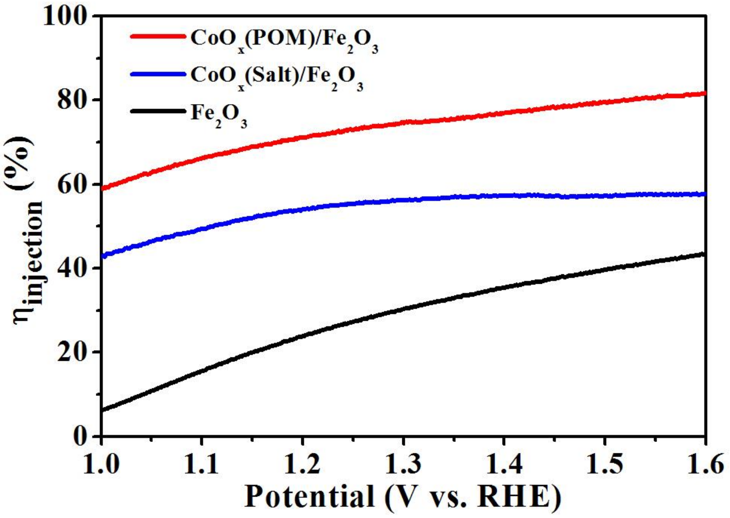

Figure S14. Charge injection efficiency ($\eta_{injection}$) of CoO$_x$(POM)/Fe$_2$O$_3$, CoO$_x$(Salt)/Fe$_2$O$_3$, and Fe$_2$O$_3$ photoanodes.

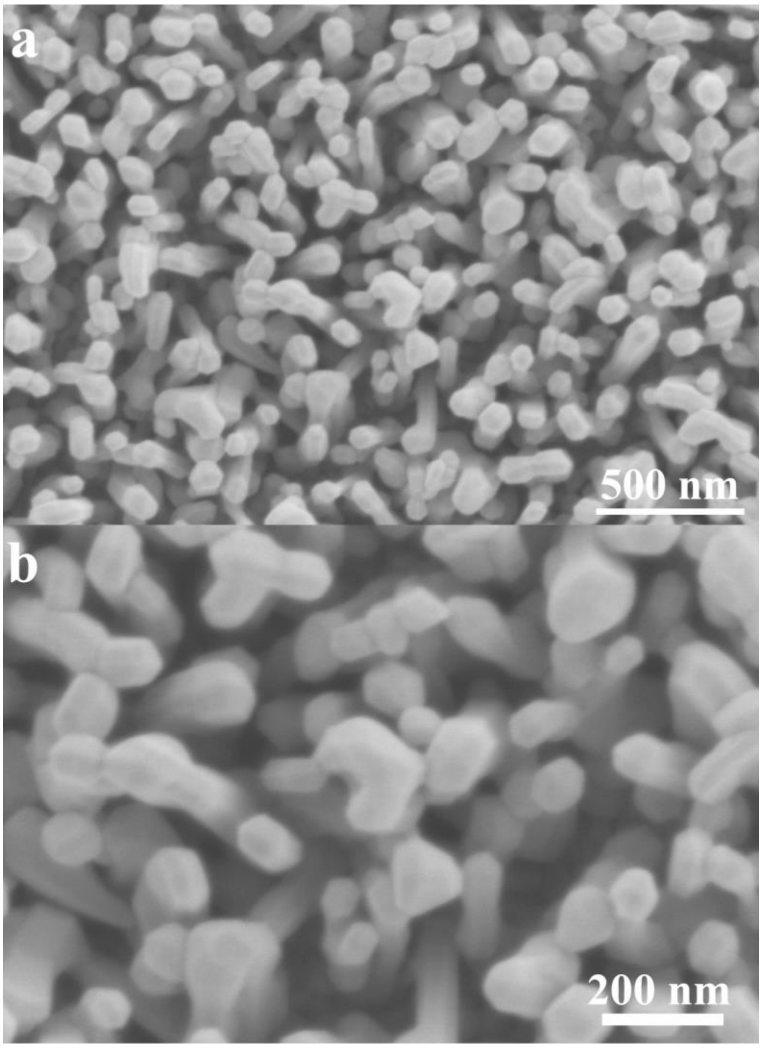

Figure S15. SEM of pristine Fe$_2$O$_3$ photoanode: (a) 500 nm (b) 200 nm.

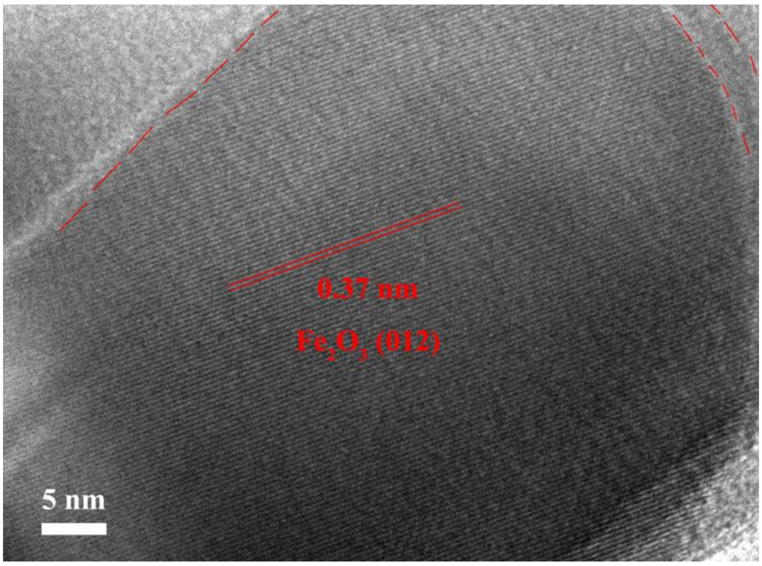

Figure S16. HRTEM of CoO_x(Salt)/Fe_2O_3 photoanode. It is considered that the cocatalyst overlayer in CoO_x(Salt)/Fe_2O_3 electrode probably consists of CoB_i and CoO_x species and has an amorphous morphology.

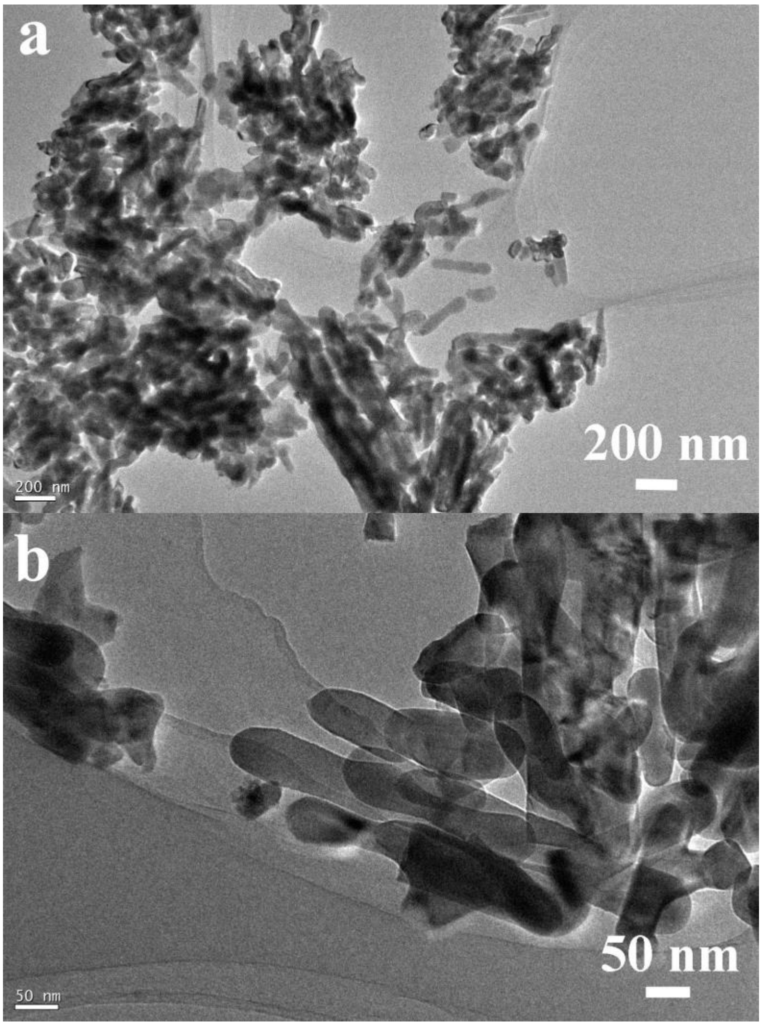

Figure S17. TEM images of CoO_x(POM)/Fe_2O_3 photoanode.

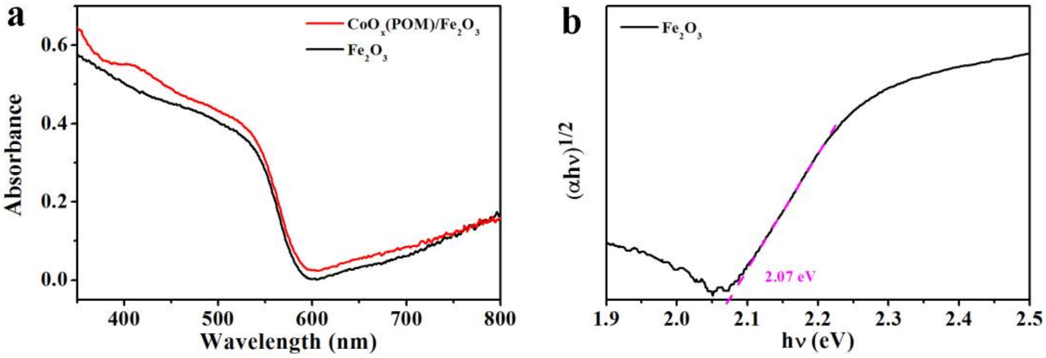

Figure S18. (a) UV-vis diffuse reflectance spectra of Fe_2O_3 and CoO_x(POM)/Fe_2O_3. (b) Tauc plot of Fe_2O_3 (estimated as 2.07 eV). Because the CoO_x layer owns an ultrathin nanostructure, a negligible increase of absorbance is observed after fabricating CoO_x overlayer on hematite photoanode.

Table S1 Comparison of our composite photoanode to other hematite photoanodes coupled Co-based cocatalysts[a)]

Catalysts	Electrolyte	J with cocatalyst	J without cocatalyst	Ratio	Fabricating method	Ref.
CoO_x(POM), Fe_2O_3 [b)]	80 mM borate buffer pH 9	1.1	0.5	2.2	PD	This work
CoO_x(Salt), Fe_2O_3 [b)]	80 mM borate buffer pH 9	0.7	0.5	1.4	PD	This work
CoO_x(POM), Fe_2O_3 [b)]	1 M NaOH pH 13.6	2.4	1.2	2.0	PD	This work
Co_3O_4, Fe_2O_3 [b)]	0.5 M KOH pH 13.43	0.64	Ca. 0.4	1.6	drop-casting	[5]
Co_3O_4, Fe_2O_3 [b)]	1 M NaOH pH 13.6	1.2	0.72	1.67	HT	[6]
Co_3O_4, Fe_2O_3 [b)]	1 M NaOH pH 13.6	1.23	0.83	Ca. 1.48	HT	[7]
CoO_x, Fe_2O_3 [b)]	1 M KOH	0.65	0.25	Ca. 2.6	ALD	[8]
CoO_x, Fe_2O_3 [c)]	0.1 M KOH pH 13.1	2.1	1.4	Ca. 1.5	ALD	[9]
Co-Pi, Fe_2O_3[b)]	1 M NaOH pH 13.6	Ca. 0.6	Ca. 0.41	Ca. 1.46	ED	[10]

a): AM 1.5G 100 mW/cm^2, b): current density at 1.23 V_{RHE} (mA/cm^2), c): current density at 1.53 V_{RHE} (mA/cm^2) PD = photodeposition method, HT = hydrothermal method, ALD = atomic layer deposition method, ED = electrodeposition method.

Table S2 Elemental composition (%) of CoO_x(POM)/Fe_2O_3, CoO_x(Salt)/Fe_2O_3, and Fe_2O_3 determined by XPS

Element	Fe_2O_3	CoO_x(POM)/Fe_2O_3	CoO_x(Salt)/Fe_2O_3	Co_8POM
B 1s	1.97	1.58	3.65	-
C 1s	49.31	46.18	44.8	40.22
Fe 2p	11.31	8.54	8.46	-
O 1s	37.41	37.96	39.39	34.79
Co 2p	-	4.63	3.7	3.57
W 4f	-	0.57	-	8.13

In a Co_8POM molecular formula ($[(A\text{-}\alpha\text{-}SiW_9O_{34})_2Co_8(OH)_6(H_2O)_2(CO_3)_3]^{16-}$), element W is more than element Co. The W/Co ratio in CoO_x(POM)/Fe_2O_3 is 0.12 while that in Co_8POM is 2.28 (ideal value is 2.25). This results confirm that Co_8POM is affected by photo-generated carriers, transforming into an ultrathin CoO_x overlayer in situ. Element Si is not representative for the reason that FTO also contains element Si. In addition, Co content of CoO_x(Salt)/Fe_2O_3 is comparable to that of CoO_x(POM)/Fe_2O_3 (in the form of Co to Fe ratio).

Table S3 Determination of metal element ratios in the POM and electrodes obtained by ICP-AES

Sample	W to Co ratio	Co to Fe ratio	B to Fe ratio
$CoO_x(POM)/Fe_2O_3$	0.18	0.15	0.37
$CoO_x(Salt)/Fe_2O_3$	-	0.25	1.12
Co_8POM	1.71	-	-
Co_8POM (ideal)	2.25	-	-

It is still observed that W is not obviously influenced by hematite (adsorption is unavoidable). In addition, Co content of $CoO_x(Salt)/Fe_2O_3$ is comparable to that of $CoO_x(POM)/Fe_2O_3$ (In order to match with the atom number of Co ions in Co_8POM molecular, a concentration of 16 μM Co^{2+} solution was used in place of 2 μM Co_8POM solution).

Table S4 Determination of metal element amount in the POM and electrodes obtained by ICP-AES (for calculating ratios in table S3)

Sample	Fe	Co	W	B
		10^{-6} mol/L		
$CoO_x(POM)/Fe_2O_3$	17.19	2.63	0.48	6.34
$CoO_x(Salt)/Fe_2O_3$	13.60	3.42	-	15.25
Co_8POM	-	1216.98	2086.33	-

The amount of each metal is detected based on a piece of photoanode sample. For ICP-AES measurements, the composite catalysts on this piece of electrode were dissolved into acid solution.

Table S5 Fitting slopes of all electrodes and calculated ratios according to the results of electrochemical active surface areas

Sample	Fitted linear slopes	Composite/pristine photoanodes ratio in slope
Pristine Fe_2O_3	0.015	1
CoO_x(POM)/Fe_2O_3	0.021	1.4
CoO_x(POM)/Fe_2O_3 after test	0.019	1.3
CoO_x(Salt)/Fe_2O_3	0.021	1.4
CoO_x(Salt)/Fe_2O_3 after test	0.016	1.1

References

[1] J. Wei, Y. Feng, P. Zhou, Y. Liu, J. Xu, R. Xiang, Y. Ding, C. Zhao, L. Fan, C. Hu, ChemSusChem 8 (2015) 2630-2634.

[2] J. Yang, H. Liu, W.N. Martens, R.L. Frost, J. Phys. Chem. C 114 (2010) 111-119.

[3] X. Zhou, J. Huang, F. Zhang, Y. Zhao, Y. Zhang, Y. Ding, Dalton Trans. 46 (2017) 10602-10610.

[4] J. Huang, Y. Zhang, Y. Ding, ACS Catal. 7 (2017) 1841-1845.

[5] J.M. Feckl, H.K. Dunn, P.M. Zehetmaier, A. Müller, S.R. Pendlebury, P. Zeller, K. Fominykh, I. Kondofersky, M. Döblinger, J.R. Durrant, C. Scheu, L. Peter, D. Fattakhova-Rohlfing, T. Bein, Adv. Mater. Interfaces 2 (2015) 1500358.

[6] L. Xi, P.D. Tran, S.Y. Chiam, P.S. Bassi, W.F. Mak, H.K. Mulmudi, S.K. Batabyal, J. Barber, J.S.C. Loo, L.H. Wong, J. Phys. Chem. C 116 (2012) 13884-13889.

[7] P. Zhang, T. Wang, X. Chang, L. Zhang, J. Gong, Angew. Chem. Int. Ed. 128 (2016) 5945 –5949.

[8] C. Du, J. Wang, X. Liu, J. Yang, K. Cao, Y. Wen, R. Chen, B. Shan, Phys. Chem. Chem. Phys. 19 (2017) 14178-14184.

[9] S.C. Riha, B.M. Klahr, E.C. Tyo, S. Seifert, S. Vajda, M.J. Pellin, T.W. Hamann, A.B.F. Martinson, ACS Nano 7 (2013) 2396–2405.

[10] D.K. Zhong, J. Sun, H. Inumaru, D.R. Gamelin, J. Am. Chem. Soc. 131 (2009) 6086-6087.